



Viscous dilation as a mechanism of magma mixing in the Ghansura Rhyolite Dome of Bathani volcano-sedimentary sequence, Eastern India

Bibhuti Gogoi ^{1,*}, Hireद्या Chauhan ², Ashima Saikia ³

¹ Department of Geology, Cotton University, Guwahati, Assam - 781001, India

² EPMA Laboratory, Department of Geology, Centre of Advanced Study, Banaras Hindu University, Varanasi - 221005, India

³ Department of Geology, University of Delhi, Delhi - 110007, India

ARTICLE INFO

Submitted: April 2020

Accepted: June 2020

Available on line: October 2020

* Corresponding author:

bibhuti.gogoi.baruah@gmail.com

DOI: 10.2451/2020PM16635

How to cite this article:

Gogoi B. et al. (2020)

Period. Mineral. 89, 285-295

ABSTRACT

The comingled mafic-felsic rocks of the Ghansura Rhyolite Dome of Bathani volcano-sedimentary sequence, Eastern India, have preserved veins of iron oxide. These veins are transporting iron oxide from the mafic zones into the adjacent felsic zones and enriching the latter with iron oxide. An interesting phenomenon displayed by the iron oxide veins is that as they travel from the mafic zones into the felsic zones, the veins undergo viscous dilation. Results presented in this work suggest that when crystal-rich mafic magma came in contact with water-rich felsic magma, amphibole present in the mafic phase got replaced by biotite along with iron oxide, calcite and quartz. The newly produced iron oxide in the mafic phase then ventured into the adjacent felsic magma as veins. As these veins ventured into the felsic phase, the similarity in viscosities between the two fluids caused the iron oxide veins to undergo viscous dilation. The onset of viscous dilation increased the interfacial area between the two fluids and enhanced mixing by facilitating chemical diffusion between them.

Keywords: viscous dilation; magma mixing; chemical diffusion; Ghansura Rhyolite Dome; Bathani volcano-sedimentary sequence.

INTRODUCTION

Crustal magma chambers are often invaded by deep-rooted mafic magmas leading to different degrees of interaction between felsic and mafic magmas (Wiebe, 1994; De Campos et al., 2004; Perugini and Poli, 2005; Gogoi et al., 2018a). Even though magma mixing is a widespread phenomenon, our understanding of the exact mechanisms governing the interaction between two dissimilar magmas remains essentially poor. Since drilling into a magma chamber is not possible with the currently available techniques, we are not in a position to directly witness the mechanisms that operate within a magma reservoir. As such, textural features preserved in magmatic rocks can play a very crucial role to understand the behavior of magmas in a magma chamber, which is

otherwise inaccessible (Gogoi et al., 2017, 2018b).

When compositionally dissimilar magmas are allowed to mix, the nature of the interaction between them is primarily controlled by their viscosity ratio (V_R). In fact, within a single magmatic system, a large gamut of viscosity ratio may prevail between the participating fluids (Perugini and Poli, 2005). Depending on the viscosity ratio, magmas may interact differently to produce a wide variety of textural features. When a low-viscosity fluid displaces a high-viscosity fluid, the mode of interaction gives rise to finger-like patterns representing Saffman-Taylor instability (Darvishi and Cubaud, 2012). The viscous fingering mechanism was well documented from the Vegetation Island outcrops of Terra Nova Intrusive Complex, Antarctica, where the mafic-felsic interfaces

display finger-like morphologies (Perugini and Poli, 2005). On the other hand, high-viscosity fluid displacing a low-viscosity fluid leads to the development of a variety of instabilities, like viscous folding (folding and coiling of viscous filaments due to longitudinal compressive stress) and Rayleigh-Plateau instability or viscous swirling (breaking up of viscous filaments into emulsions due to capillary force; Cubaud and Mason, 2006; Chung et al., 2010; Darvishi and Cubaud, 2012). The phenomenon of viscous folding was highlighted from the mingled rocks of Ghansura Rhyolite Dome (GRD) within the Bathani volcano-sedimentary sequence (Gogoi and Saikia, 2018) and from the migmatites of Chotanagpur Granite Gneiss Complex (Gogoi et al., 2020a). Furthermore, the mechanism of viscous swirling was documented from the non-porphyrific hybrid rocks of GRD (Gogoi and Saikia, 2019). Here, we investigate the occurrence of viscous dilation preserved in the mingled rocks of GRD. Similar to the other physical phenomena discussed earlier, the phenomenon of viscous dilation may be a powerful tool to facilitate mixing between two physically and chemically distinct magmas.

Recent developments in microfluidics have improved our understanding of the mixing between viscous fluids at the small scale. The experiments involving viscous dilation are executed in a microfluidic apparatus at normal room temperature, wherein viscous fluids like ethanol and silicone oils are used (Mason, 2008; Cubaud et al., 2011). In these experiments, a thin filament of a viscous fluid is allowed to pass through a different outer fluid by hydrodynamic focusing in the microfluidic apparatus. If the viscosity of the fluid propagating as filament is similar to that of the outer fluid, the thread simply dilates representing viscous dilation. Thus, viscous dilation may be a unique mechanism to mix two fluids whose viscosities are similar. The existence of viscous dilation in the mingled rocks of GRD gives us a unique opportunity to better understand the nature of interaction between basaltic and rhyolitic magmas at the small scale.

GEOLOGICAL SETTING AND FIELD RELATIONS

The Bathani volcano-sedimentary sequence (BVSS) is a bimodal volcanic suite situated in the northern fringe of the Chotanagpur Granite Gneiss Complex (CGGC), Eastern India (Figure 1). An island-arc setting was proposed for the evolution of the Bathani volcanics (Saikia et al., 2014, 2017, 2019; Gogoi et al., 2020b). The volcano-sedimentary suite of rocks may be broadly classified into three litho-units (Ahmad and Wanjari, 2009): a) mafic volcanics comprising pillow basalt and mafic pyroclasts b) felsic volcanics comprising rhyolite c) volcano-sedimentary sequence comprising tuff, dolomite, banded chert and banded iron formation. The Ghansura Rhyolite

Dome together with some minor emplaced granitic bodies in the form of small hillocks and plutons are seen cross-cutting or overlying the volcano-sedimentary sequence.

The present work was carried out in a small rhyolite dome located near Ghansura village in the Indian state of Bihar. The rhyolite dome is a part of the Bathani volcano-sedimentary sequence (Figure 1) that preserves evidence of mafic-felsic magma interactions at the outcrop scale. The Ghansura Rhyolite Dome was a partly solidified subvolcanic felsic magma chamber that was intruded by basaltic magma during its evolution leading to the formation of a wide variety of hybrid rocks (Gogoi et al., 2018b). The hybrid rocks encountered in the rhyolite dome include:

a) Intermingled mafic-felsic rocks with well-defined reaction surface (Figure 2a).

b) Non-porphyrific intermediate rock displaying emulsion texture (Figure 2b). This hybrid rock is characterized by a fine comingled texture, in which millimeter-sized darker mafic spherical to sub-spherical globules are engulfed in a fine-grained homogeneous groundmass (Gogoi and Saikia, 2019).

c) Porphyritic intermediate rock displaying rapakivi texture (Figure 2c). Unlike the intermingled mafic-felsic rocks, this hybrid rock appears to be a homogeneous product of magma mixing as individual entities of the parental mafic and felsic magmas could not be traced in this rock.

d) Mafic rocks containing felsic clasts (Figure 2d) and felsic microgranular enclaves/felsic ocelli. The preservation of angular clasts in the mafic rocks suggests that some portions of the felsic magma chamber were already solidified when mafic magma disrupted it (Gogoi et al., 2018b; Gogoi et al., 2020b).

PETROGRAPHY

The rocks of the GRD may be broadly divided into three distinct categories: a) basalts b) rhyolites c) hybrid rocks.

Basalts

These rocks constitute the mafic end-member of our study domain. They consist of clinopyroxene (45-55 vol%), plagioclase (35-40 vol%) and Ti-Fe oxide (5-10 vol%) as major phases, while amphibole and biotite constitute the minor phases. Clinopyroxene occurs as large anhedral to subhedral grains showing weak pleochroism from colorless to pale brown. It is identified by its high relief and shows second to third order interference colors. It shows inclined extinction with some grains showing one set of cleavage. Clinopyroxene occurs as phenocrysts in the rock depicting porphyritic texture. Plagioclase occurs as small-to-medium sized grains having anhedral to subhedral form. It is identified by its low relief and first

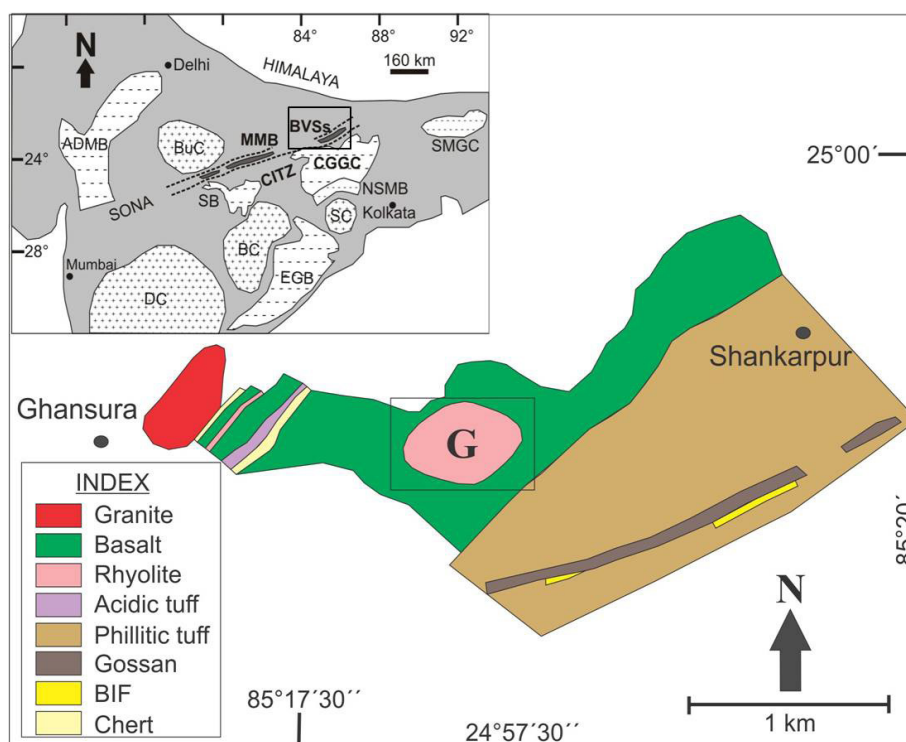


Figure 1. A simplified geological map of the Bathani volcano-sedimentary sequence (BVSSs). The Ghansura Rhyolite Dome is marked within the black rectangle and is represented as 'G' (reproduced after Gogoi and Saikia, 2018). Inset shows the location of BVSSs together with other Proterozoic mobile belts of India. Also shown are four Archean cratonic nuclei, namely Singhbhum (SC), Bastar (BC), Bundelkhand (BuC) and Dharwar (DC; modified after Chatterjee and Ghosh, 2011). Abbreviations: CITZ - Central Indian Tectonic Zone, EGB - Eastern Ghats Belt, ADMB - Aravalli Delhi Mobile Belt, CGGC - Chotanagpur Granite Gneiss Complex, SB - Satpura Belt, MMB - Mahakoshal Mobile Belt, SMGC - Shillong-Meghalaya Gneissic Complex, NSMB - North Singhbhum Mobile Belt and SONA - Son-Narmada Lineament.

order grey interference color and characteristic lamellar twinning. Laths of euhedral plagioclase are enclosed within clinopyroxene phenocrysts depicting ophitic texture (Figure 3a). Ti-Fe oxide occurs as subhedral to euhedral grains with high relief and appears dark in color. Amphibole and biotite are present in very low concentrations in these rocks and usually occur as altered products of primary clinopyroxene.

Rhyolites

These rocks represent the felsic end-member of our study domain. They are fine-grained with the mineral grains mostly ranging from subhedral to anhedral in shape (Figure 3b). The mineralogical assemblage identified in this rock includes quartz, K-feldspar, muscovite and Fe-oxide. The minerals constituting these fine-grained rocks have been confirmed from EPMA analyses (Saikia et al., 2014).

Comingled mafic-felsic rocks

As already been discussed earlier, four different

varieties of hybrid rocks are encountered in the study domain. For the present work, we focus our petrographical observations only on the comingled mafic-felsic rocks (Figure 2a).

This variety of hybrid rock is fine-to-medium grained and essentially consists of amphibole (20-30 vol%), biotite (20-25 vol%), quartz (10-15 vol%), plagioclase (10-15 vol%), K-feldspar (5-10 vol%), ilmenite (5-10 vol%), calcite (<5 vol%), titanite (<5 vol%) and muscovite (<5 vol%). Two distinct zones in contact with each other have been identified in thin section: a) medium-grained mafic zones with amphibole, biotite, plagioclase, ilmenite, titanite, calcite and quartz, and b) fine-grained felsic zones with quartz, K-feldspar, muscovite, biotite and ilmenite. Amphibole occurs as anhedral to subhedral grains and shows strong pleochroism from light green to dark green. It is identified by moderate relief and second order interference color. Biotite occurs as small-to-medium sized grains with anhedral to subhedral form. It shows pleochroism from light brown to dark brown and is characterized by high order interference colors.

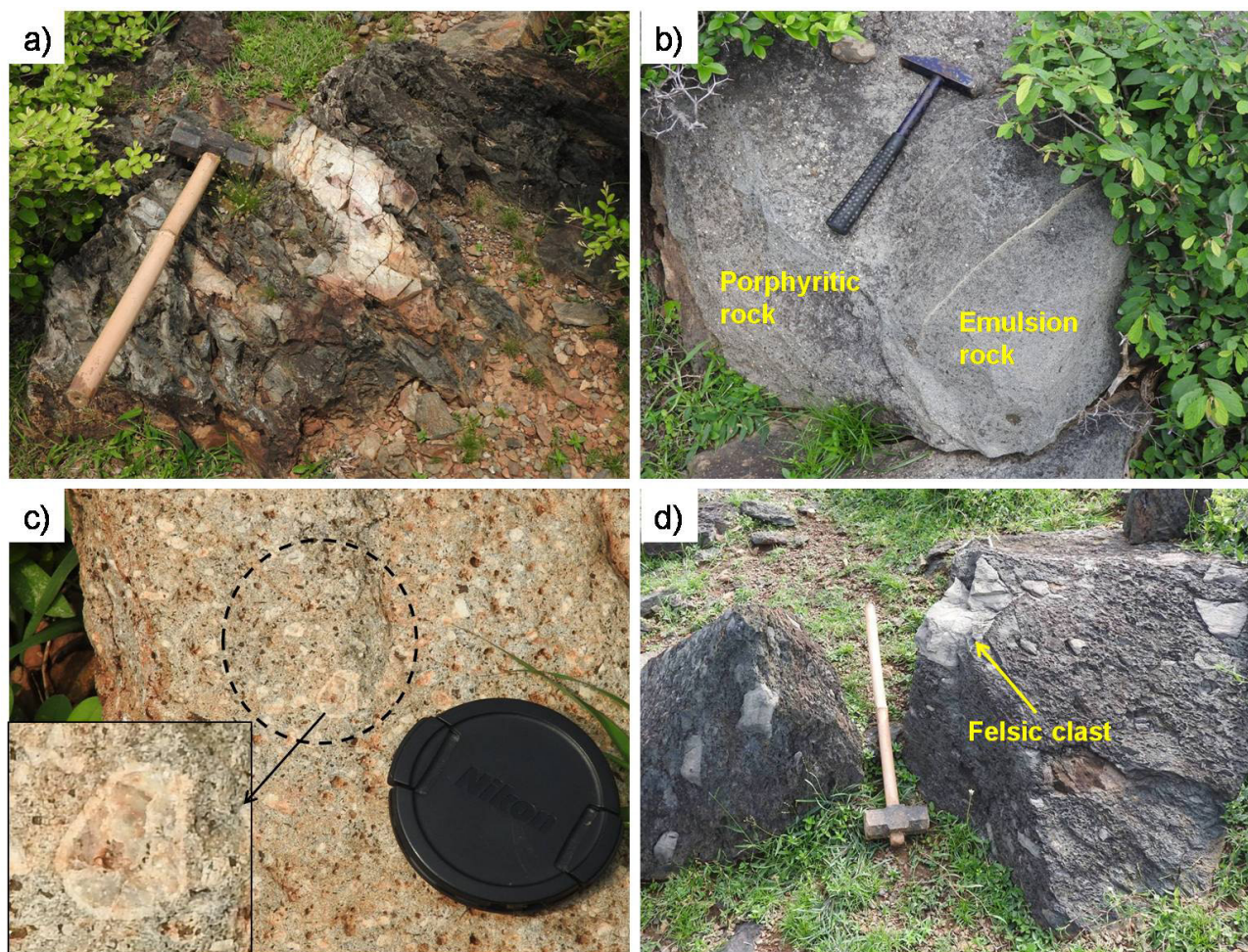


Figure 2. Field photographs displaying (a) Comingled mafic-felsic rocks. (b) Non-porphyrific intermediate rock with emulsions in contact with the porphyritic intermediate rock. (c) Porphyritic intermediate rock with rapakivi feldspars (inset shows a magnified rapakivi feldspar). A few rapakivi feldspars are marked within the dashed circle. (d) Mafic rocks with felsic clasts.

Plagioclase occurs as small anhedral grains having low relief and display first order grey interference color. Quartz, K-feldspar and muscovite mostly occur as fine-grained groundmass in the felsic zones. Petrographic observations have revealed that biotite, ilmenite, titanite and calcite are altered products of amphibole (Figure S1). It is to be noted here that quartz is also present as an altered product of amphibole in this rock (Figure S1c).

A distinctive attribute of this section is the existence of veinlets of individual minerals like biotite and ilmenite. These veins appear to be travelling from the mafic zones into the felsic zones. A notable feature about the biotite veins is that closer to the mafic zones where they originate, the veins are constituted by amphibole rather than biotite and as they migrate from the mafic zones into the felsic zones amphibole gets replaced by biotite (Figure 3c). Veins of ilmenite are also observed migrating from the

mafic zones into the felsic zones.

An important feature about the biotite and iron oxide veins is that these veins are frequently exhibiting flow instabilities. The biotite veins display folding or buckling instability as they propagate through the felsic zones depicting viscous folding (Figure 3c). On the other hand, the veins of iron oxide are getting dilated as they enter into the felsic zones from the mafic zones depicting viscous dilation (Figure 3 d-f).

ANALYTICAL METHODS

The mineral analyses were carried out on the Electron Probe Micro Analyzer (EPMA) CAMECA SX Five instrument at DST-SERB National Facility, Department of Geology (Center of Advanced Study), Institute of Science, Banaras Hindu University. Polished thin sections were coated with 20 nm thin layer of carbon for electron probe

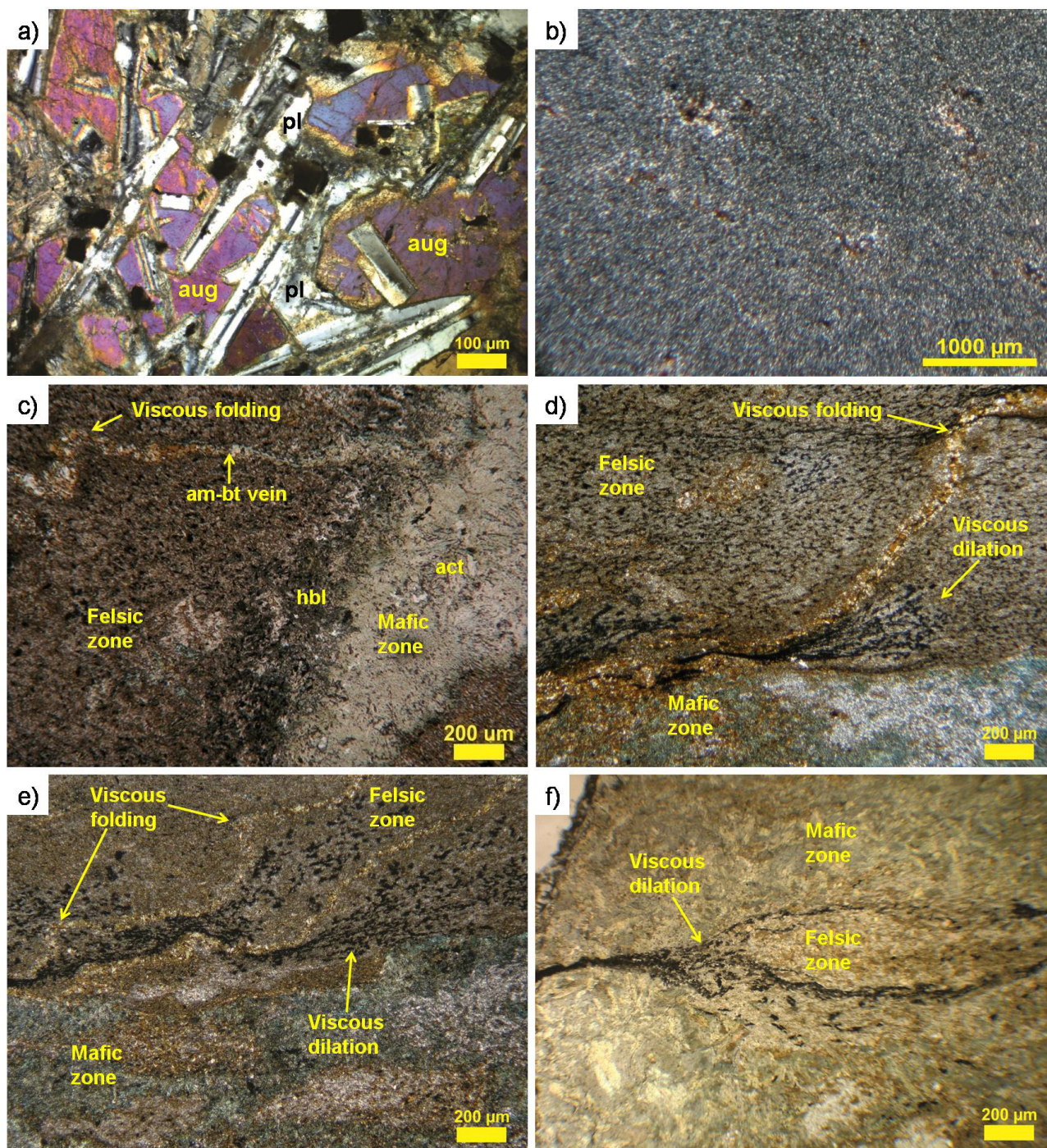


Figure 3. Photomicrographs displaying (a) Ophitic texture in the basaltic rocks. (b) CPL view of the fine-grained rhyolite. (c) An amphibole-biotite vein displaying viscous folding. (d-f) Veins of iron oxide displaying viscous dilation. Mineral abbreviations: act = actinolite, am = amphibole, aug = augite, bt = biotite, hbl = hornblende, pl = plagioclase

microanalyses using LEICA-EM ACE200 instrument. The CAMECA SX Five instrument was operated by SX Five Software at a voltage of 15 kV and current of 10 nA with a LaB₆ source in the electron gun for the generation

of the electron beam. Natural silicate mineral andradite was used as an internal standard to verify positions of crystals (SP1-TAP, SP2-LiF, SP3-LPET, SP4-LTAP and SP5-PET) for corresponding wavelength dispersive (WD)

spectrometers (SP#) in CAMECA SX-Five instrument. The following X-ray lines were used in the analyses: F-K α , Na-K α , Mg-K α , Al-K α , Si-K α , P-K α , Cl-K α , K-K α , Ca-K α , Ti-K α , Cr-K α , Mn-K α , Fe-K α , Ni-K α and Ba-L α . Natural mineral standards: fluorite (F), halite (Cl), periclase (Mg), diopside (Ca), corundum (Al), wollastonite (Si), apatite (P), orthoclase (K), albite (Na), rutile (Ti), chromite (Cr), Rhodonite (Mn), hematite (Fe) and barite (Ba); Ni pure metal standard supplied by CAMECA-AMETEK used for routine calibration and quantification. Routine calibration, acquisition, quantification and data processing were carried out using SxSAB version 6.1 and SX-Results software of CAMECA. The precision of the analysis is better than 1% for major element oxides and 5% for trace elements from the repeated analysis of standards.

MINERAL CHEMISTRY

Mineral chemical analyses were carried out exclusively on the iron oxide veins displaying viscous dilation and iron oxide from the adjoining felsic zones. Backscattered electron images of an iron oxide vein displaying viscous dilation are shown in Figure 4. Representative analyses of iron oxide from the veins and adjacent felsic groundmass are presented in Table 1. Mineral chemical compositions

obtained by EPMA disclose that the iron oxide contains 31.90 wt% to 43.41 wt% FeO(t), 2.04-4.02 wt% MnO and traces of MgO, while TiO₂ content varies between 38.92-53.66 wt%. The calculated Fe₂O₃ content remains below 4 wt%. The Fe₂O₃ calculation was done following the Fe_{tot} recalculation method of Droop (1987). End-member compositions of iron oxide were calculated based on six oxygens. In the TiO₂-FeO-Fe₂O₃ classification diagram (Figure 5 a,b), the iron oxides from the veins and felsic groundmass plot close to the ideal composition of ilmenite.

DISCUSSION

The whole-rock chemistry and mineral compositions of the major mineral phases from the putative mafic and felsic endmembers and their hybrid products have already been reported from the GRD (Gogoi and Saikia, 2018; Gogoi et al., 2018b; Gogoi and Saikia, 2019). Moreover, compositions of the major mineral phases from the mingled rocks displaying viscous dilation can be found in Gogoi and Saikia (2018). In this work, we are entirely focusing on the iron oxide veins and the physical phenomenon displayed by these veins.

The comingled mafic-felsic rocks of the GRD have preserved mineral veins that appear to be transporting

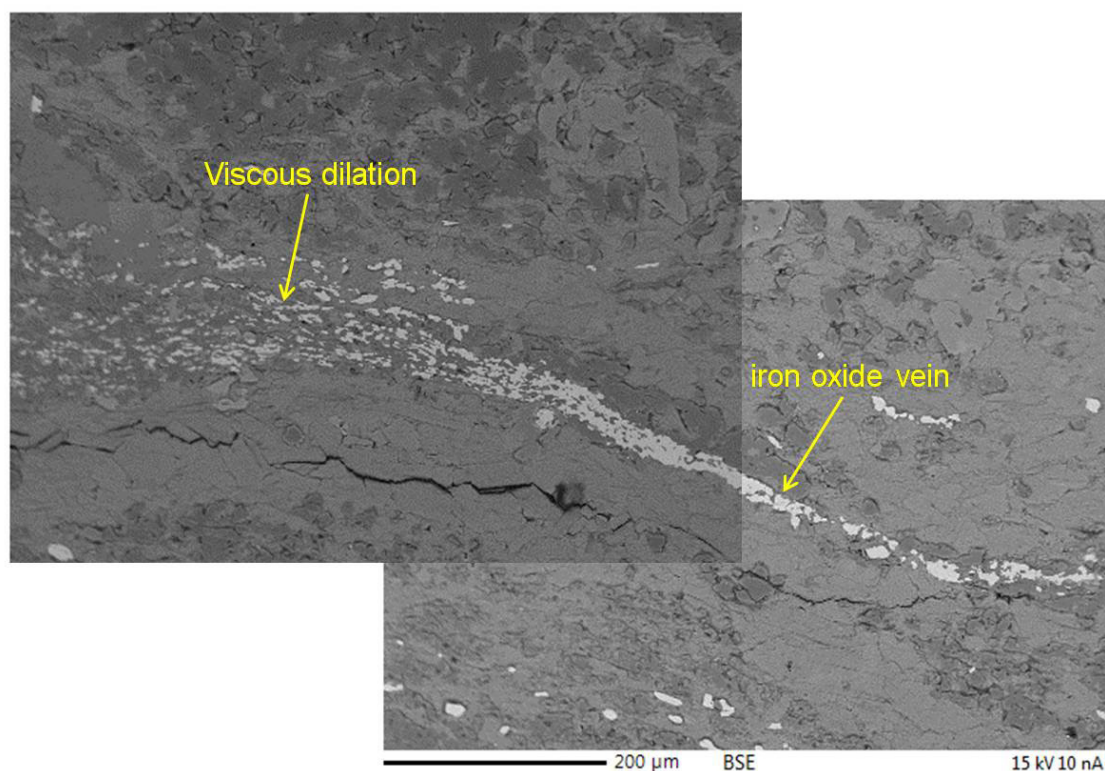


Figure 4. Backscattered electron images showing an iron oxide vein undergoing viscous dilation.

Table 1. Representative EPMA analyses of iron oxide from the comingled mafic-felsic rocks of Ghansura Rhyolite Dome.

Location	iron oxide vein															
SiO ₂	0.05	0.75	0.02	0.33	3.72	0.49	8.91	0.64	2.47	0.34	0.12	0.46	0.02	0.12	0.07	0.43
TiO ₂	53.00	52.33	52.75	51.46	47.10	51.34	48.07	53.03	50.13	49.62	52.94	52.57	52.98	52.01	52.58	51.43
Al ₂ O ₃	0.00	0.43	0.02	0.03	0.36	0.14	2.05	0.22	0.57	1.91	0.13	0.46	0.00	0.00	0.00	0.18
FeO	42.64	40.71	42.42	42.42	36.76	41.53	31.90	41.01	40.53	40.24	40.03	40.81	40.77	42.46	42.05	41.71
MnO	3.24	3.58	3.70	3.42	3.00	3.40	2.51	3.93	3.79	2.98	3.47	3.80	3.93	3.24	3.23	3.70
MgO	0.07	0.10	0.06	0.13	0.12	0.17	0.08	0.19	0.10	1.13	0.44	0.05	0.03	0.16	0.12	0.15
CaO	0.11	0.92	0.11	0.98	6.47	0.85	6.18	0.21	0.32	0.26	0.20	0.21	0.22	0.51	0.69	1.20
Total	99.11	98.82	99.08	98.78	97.53	97.92	99.70	99.23	97.91	96.48	97.35	98.36	97.95	98.50	98.75	98.79
Calculation based on 6 O																
Si	0.00	0.04	0.00	0.02	0.19	0.02	0.43	0.03	0.13	0.02	0.01	0.02	0.00	0.01	0.00	0.02
Ti	2.03	2.00	2.02	1.97	1.77	1.98	1.74	2.02	1.92	1.91	2.06	2.02	2.06	2.00	2.02	1.96
Al	0.00	0.03	0.00	0.00	0.02	0.01	0.12	0.01	0.03	0.12	0.01	0.03	0.00	0.00	0.00	0.01
Fe ³⁺	0.00	0.00	0.00	0.03	0.06	0.00	0.00	0.00	0.00	0.02	0.00	0.00	0.00	0.00	0.00	0.02
Fe ²⁺	1.82	1.73	1.81	1.77	1.48	1.78	1.29	1.74	1.73	1.70	1.73	1.75	1.76	1.81	1.79	1.75
Mn	0.14	0.15	0.16	0.15	0.13	0.15	0.10	0.17	0.16	0.13	0.15	0.16	0.17	0.14	0.14	0.16
Mg	0.01	0.01	0.00	0.01	0.01	0.01	0.01	0.01	0.01	0.09	0.03	0.00	0.00	0.01	0.01	0.01
Ca	0.01	0.05	0.01	0.05	0.35	0.05	0.32	0.01	0.02	0.01	0.01	0.01	0.01	0.03	0.04	0.07
Total	4.00	4.00	4.00	4.00	4.00	4.00	4.00	4.00	4.00	4.00	4.00	4.00	4.00	4.00	4.00	4.00

mineral phases from the mafic zones to the felsic zones. This distribution of minerals between the mafic-felsic zones displays a unique mechanism of interaction between the contrasting magmas. Another important observation in this rock is the demonstration of flow instabilities by the mineral transporting veins. The amphibole-biotite veins frequently display buckling or folding instability (Figure 3 c-e) as they travel from the mafic zones into the felsic zones, while the iron oxide veins display viscous dilation as they move from the mafic zones into the felsic zones (Figure 3 d-f). Mixing between two fluids with different viscosities can be enhanced by flow instabilities that bring about heterogeneity and disorder in the flow (Jha et al., 2011). The fundamental principle behind fluid mixing is that flow instabilities increase fluid-fluid interfacial area and enhance mixing by chemical diffusion (De Campos et al., 2011; Morgavi et al., 2013, Gogoi et al., 2020a). A variety of flow instabilities exist that may operate depending on the viscosity difference between two fluids. When a thread of high viscosity fluid propagates through

a low viscosity fluid, the thread may undergo Rayleigh-Plateau instability (fragmentation of the fluid filament into droplets or emulsions due to the action of capillary force), coalescence (amalgamation between droplets) or viscous folding (folding and buckling of the high viscosity thread due to the action of compressive stress). However, when a low viscosity fluid displaces a high viscosity fluid, it leads to the development of Saffman-Taylor instabilities or viscous fingering. Furthermore, when a thread of a viscous fluid is allowed to pass through another fluid with similar viscosity, the thread simply dilates (Mason, 2008; Cubaud et al., 2011). The phenomenon of viscous dilation increases the contact area between the two fluids enhancing mixing between them by chemical diffusion. The iron oxide veins preserved in the mingled rocks of our study area display viscous dilation. These veins remain as a single filament in the mafic zones, but as soon as they enter into the felsic zones, the veins simply dilate. This is a strong indication that the viscosities of the iron oxide melt and the magma constituting the felsic zones

Table 1. ...Continued

Location	iron oxide vein															
SiO ₂	0.56	2.68	2.03	0.08	0.06	0.00	0.48	0.43	0.07	0.91	0.07	0.02	0.60	0.13	0.12	0.11
TiO ₂	48.63	50.25	51.64	51.97	52.90	52.98	52.55	52.20	53.19	52.09	53.56	53.02	52.20	51.71	53.43	53.23
Al ₂ O ₃	0.00	0.63	0.04	0.00	0.00	0.01	0.22	0.36	0.00	0.26	0.00	0.00	0.00	0.03	0.00	0.00
FeO	40.92	39.08	41.62	41.76	40.29	41.71	40.63	38.36	40.57	40.29	39.75	40.60	41.04	41.37	40.93	40.95
MnO	3.00	3.32	3.43	3.40	3.27	3.46	3.16	3.28	4.02	3.58	3.59	3.57	3.66	3.42	3.56	4.02
MgO	0.15	0.15	0.06	0.09	0.08	0.06	0.09	0.26	0.05	0.04	0.00	0.02	0.02	0.08	0.07	0.04
CaO	2.88	5.26	1.63	0.53	0.31	0.36	0.34	0.81	0.22	0.80	0.19	0.18	0.24	0.41	0.15	0.14
Total	96.15	101.36	100.44	97.83	96.92	98.59	97.46	95.70	98.12	97.96	97.16	97.41	97.76	97.15	98.25	98.48
Calculation based on 6 O																
Si	0.03	0.13	0.10	0.00	0.00	0.00	0.02	0.02	0.00	0.05	0.00	0.00	0.03	0.01	0.01	0.01
Ti	1.89	1.83	1.93	2.01	2.07	2.04	2.04	2.06	2.06	2.01	2.10	2.07	2.02	2.02	2.07	2.05
Al	0.00	0.04	0.00	0.00	0.00	0.00	0.01	0.02	0.00	0.02	0.00	0.00	0.00	0.00	0.00	0.00
Fe ³⁺	0.15	0.04	0.00	0.00	0.00	0.00	0.00	0.00	0.00	0.00	0.00	0.00	0.00	0.00	0.00	0.00
Fe ²⁺	1.62	1.54	1.73	1.80	1.76	1.79	1.76	1.68	1.75	1.73	1.73	1.76	1.77	1.79	1.76	1.76
Mn	0.13	0.14	0.14	0.15	0.14	0.15	0.14	0.15	0.18	0.16	0.16	0.16	0.16	0.15	0.15	0.17
Mg	0.01	0.01	0.00	0.01	0.01	0.00	0.01	0.02	0.00	0.00	0.00	0.00	0.00	0.01	0.01	0.00
Ca	0.16	0.27	0.09	0.03	0.02	0.02	0.02	0.05	0.01	0.04	0.01	0.01	0.01	0.02	0.01	0.01
Total	4.00	4.00	4.00	4.00	4.00	4.00	4.00	4.00	4.00	4.00	4.00	4.00	4.00	4.00	4.00	4.00

in the comingled mafic-felsic rocks were similar. Had the viscosities of the two melts were different, they would have not displayed viscous dilation. This can be verified from Figures 3d and 3e. In both the figures, it can be seen that the iron oxide veins are displaying viscous dilation, while the biotite veins are displaying viscous folding. The reason behind the demonstration of viscous folding by the biotite veins is that the viscosities of these veins were higher than the viscosity of the melt constituting the felsic zones (Gogoi and Saikia, 2018). Both biotite and iron oxide veins were products of the mafic magma, but because of their difference in viscosities, they interacted differently with the felsic magma. Ideally, mafic magmas are less viscous than felsic magmas. Under such circumstances, the mafic veins should have exhibited viscous fingering in the felsic zones (Perugini and Poli, 2005). However, viscosities of magmas are dependent on several factors like their composition, temperature, degree of crystallinity and water content. A wide range of viscosity ratios can exist between mafic and felsic magmas in a magma mixed

system (Perugini and Poli, 2005). The demonstration of viscous dilation and viscous folding by the mafic veins indicate that the viscosities of the magmas constituting these veins were similar or higher than the viscosity of the magma that produced the felsic zones.

The existence of numerous iron oxide veins in the mafic zones of the mingled rocks is intriguing. The mafic zones constituting the comingled rocks primarily consist of amphibole. Amphiboles occurring at the interior of these mafic zones are pale green in color, while those occurring at the margins appear green to dark green (Figure 3c). Mineral chemical analyses have revealed that the interior amphiboles are actinolite, while the exterior amphiboles are hornblende in composition (Gogoi and Saikia, 2018). Such compositional variations in amphiboles suggest that the mafic zones were interacting with the adjacent felsic zones. The occurrence of actinolite in the mafic zones indicates that these amphibole-rich zones were formed by solid-state reaction from clinopyroxene, as there is no experimental evidence for the crystallization

Table 1. ...Continued

Location	iron oxide vein											felsic groundmass				
SiO ₂	0.07	0.03	0.00	0.04	0.14	0.04	1.81	0.05	0.40	0.67	0.06	5.16	0.35	8.94	0.57	0.13
TiO ₂	52.97	53.35	52.67	53.40	52.53	53.52	49.52	53.22	52.04	52.74	52.24	51.23	52.25	38.92	53.66	52.09
Al ₂ O ₃	0.00	0.00	0.00	0.00	0.01	0.00	1.00	0.02	0.09	0.00	0.00	0.31	0.12	8.17	0.50	0.00
FeO	42.62	43.41	41.26	43.08	40.17	41.89	38.73	39.63	41.68	41.74	42.01	30.04	40.35	36.06	39.19	42.67
MnO	3.07	3.67	3.18	3.36	3.54	3.97	3.14	3.66	3.77	3.74	3.37	2.87	3.16	2.33	3.56	3.25
MgO	0.07	0.02	0.02	0.01	0.07	0.05	0.76	0.04	0.07	0.09	0.14	0.04	0.20	2.02	0.07	0.18
CaO	0.07	0.19	0.50	0.24	0.84	0.36	1.40	0.47	1.15	0.83	0.86	9.54	0.16	0.63	0.72	0.55
Total	98.88	100.66	97.64	100.13	97.29	99.83	96.37	97.09	99.18	99.80	98.67	99.21	96.59	97.08	98.27	98.86

Calculation based on 6 O																
Si	0.00	0.00	0.00	0.00	0.01	0.00	0.09	0.00	0.02	0.03	0.00	0.25	0.02	0.43	0.03	0.01
Ti	2.03	2.01	2.05	2.02	2.05	2.03	1.91	2.08	1.98	2.00	2.00	1.88	2.05	1.40	2.07	1.99
Al	0.00	0.00	0.00	0.00	0.00	0.00	0.06	0.00	0.01	0.00	0.00	0.02	0.01	0.46	0.03	0.00
Fe ³⁺	0.00	0.00	0.00	0.00	0.00	0.00	0.00	0.00	0.00	0.00	0.00	0.00	0.00	0.00	0.00	0.00
Fe ²⁺	1.82	1.82	1.78	1.82	1.74	1.77	1.66	1.72	1.76	1.76	1.79	1.23	1.76	1.44	1.68	1.82
Mn	0.13	0.16	0.14	0.14	0.16	0.17	0.14	0.16	0.16	0.16	0.15	0.12	0.14	0.09	0.15	0.14
Mg	0.01	0.00	0.00	0.00	0.01	0.00	0.06	0.00	0.01	0.01	0.01	0.00	0.02	0.14	0.01	0.01
Ca	0.00	0.01	0.03	0.01	0.05	0.02	0.08	0.03	0.06	0.04	0.05	0.50	0.01	0.03	0.04	0.03
Total	4.00	4.00	4.00	4.00	4.00	4.00	4.00	4.00	4.00	4.00	4.00	4.00	4.00	4.00	4.00	4.00

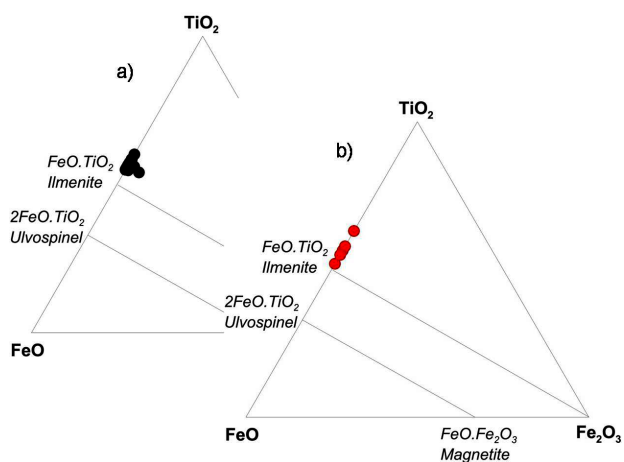
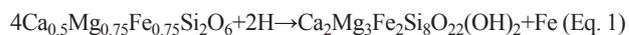


Figure 5. TiO₂–FeO–Fe₂O₃ classification diagram for iron oxide compositions (redrawn after Sassi et al., 2004). Fe₂O₃ calculated following Droop (1987). (a) Compositions of iron oxide from the veins. (b) Compositions of iron oxide from the felsic groundmass.

of actinolitic amphibole directly from the melt (Stephens, 2001). Earlier works have confirmed that the pyroxene occurring in the basaltic rocks of GRD are clinopyroxene (Gogoi and Saikia, 2018; Gogoi and Saikia, 2019). From these observations, it can be inferred that when basaltic magma containing clinopyroxene crystals came in contact with the felsic magma, diffusion of elements took place between the two contrasting magmas. The diffusion of volatiles and H⁺ ions from the felsic magma to the mafic magma promoted the formation of actinolite from early-magmatic clinopyroxene in a solid-state reaction (Castro and Stephens, 1992; Gogoi and Saikia, 2019). The chemical reaction between precursor clinopyroxene and hydrogen leading to the formation of actinolite may be written as:



(clinopyroxene)

(actinolite)

- Gogoi B., Saikia A., Ahmad M., 2018a. Field evidence, mineral chemical and geochemical constraints on mafic-felsic magma interactions in a vertically zoned magma chamber from the Chotanagpur Granite Gneiss Complex of Eastern India. *Chemie der Erde* 78, 78-102.
- Gogoi B., Saikia A., Ahmad M., Ahmad T., 2018b. Evaluation of magma mixing in the subvolcanic rocks of Ghansura Felsic Dome of Chotanagpur Granite Gneiss Complex, eastern India. *Mineralogy and Petrology* 112, 393-413.
- Gogoi, B., Chauhan, H., Hazarika, G., Baruah, A., Saikia, M., Hazarika, P.J., 2020a. Significance of viscous folding in the migmatites of Chotanagpur Granite Gneiss Complex, eastern India. *Earth and Environmental Science Transactions of the Royal Society of Edinburgh*. doi:10.1017/S1755691020000067.
- Gogoi, B., Saikia, A., Ahmad, M., 2020b. Mafic-felsic magma interactions in the Bathani volcanic-plutonic complex of Chotanagpur Granite Gneiss Complex, eastern India: implications for assembly of the Greater Indian Landmass during the Proterozoic. *Episodes* 43, 785-810.
- Goldsmith, J.R., 1987. Al/Si interdiffusion in albite: effect of pressure and the role of hydrogen. *Contributions to Mineralogy and Petrology* 95, 311-321.
- Jha B., Cueto-Felgueroso L., Juanes R., 2011. Fluid mixing from viscous fingering. *Physical Review Letters* 106, 194502.
- Mason T., 2008. Folding and swirling instabilities of viscous fluid threads in microchannels. Abstract for an Invited Paper for the MAR08, Meeting of The American Physical Society.
- Mongkoltip, P. and Ashworth, R., 1983. Exsolution of ilmenite and rutile in hornblende. *American Mineralogist* 68, 143-155.
- Morgavi, D., Perugini, D., De Campos, C.P., Ertel-Ingrisch, W., Dingwell, D.B., 2013. Time evolution of chemical exchanges during mixing of rhyolitic and basaltic melts. *Contributions to Mineralogy and Petrology* 166, 615-638.
- Perugini D. and Poli G., 2005. Viscous fingering during replenishment of felsic magma chambers by continuous inputs of mafic magmas: field evidence and fluidmechanics experiments. *Geology* 33, 5-8.
- Saikia A., Gogoi B., Ahmad M., Ahmad T., 2014. Geochemical constraints on the evolution of mafic and felsic rocks in the Bathani volcano-sedimentary sequence of Chotanagpur Granite Gneiss Complex. *Journal of Earth System Science* 123, 959-987.
- Saikia A., Gogoi B., Kaulina T., Lialina L., Bayanova T., Ahmad M., 2017. Geochemical and U-Pb zircon age characterization of Granites of Bathani volcano sedimentary sequence, Chotanagpur Granite Gneiss Complex, eastern India: vestiges of Nuna supercontinent in Central Indian Tectonic Zone. *Geological Society of London Special Publications* 457, 233-252.
- Saikia A., Gogoi B., Ahmad M., Kumar R., Kaulina T., Bayanova T., 2019. Mineral Chemistry, Sr-Nd Isotope Geochemistry and Petrogenesis of the Granites of Bathani Volcao-Sedimentary Sequence from the Northern Fringe of Chotanagpur Granite Gneiss Complex of Eastern India. In *Geological Evolution of the Precambrian Indian Shield: Society of Earth Scientists Series (M.E.A. Mondal, Eds.)*. Springer, Cham (79-120).
- Sassi R., Mazzoli C., Spiess R., Cester T., 2004. Towards a better understanding of the fibrolite problem: the effect of reaction overstepping and surface energy anisotropy. *Journal of Petrology* 45, 1467-1479.
- Stephens, W.E., 2001. Polycrystalline amphibole aggregates (clots) in granites as potential I-type restite: An ion microprobe study of rare-earth distributions. *Australian Journal of Earth Sciences* 48, 591-601.
- Vernon, R.H., 1984. Microgranitoid enclave in granite-globules of hybrid magma quenched in plutonic environment. *Nature* 309, 438-439.
- Wiebe R.A., 1994. Silicic magma chambers as traps for basaltic magmas: The Cadillac Mountain intrusive complex, Mount Desert Island, Maine. *The Journal of Geology* 102, 423-437.



This work is licensed under a Creative Commons Attribution 4.0 International License CC BY. To view a copy of this license, visit <http://creativecommons.org/licenses/by/4.0/>

